IEEE Access
Multidisciplinary | Rapid Review | Open Access Journal

Received March 10, 2019, accepted March 14, 2019, date of publication March 20, 2019, date of current version April 3, 2019.

Digital Object Identifier 10.1109/ACCESS.2019.2906340

A Reconfigurable Filter Using Defected Ground Structure for Wideband Common-Mode Suppression

ZHIBIN ZENG[1], SHENGJIAN JAMMY CHEN[2], (Member, IEEE), AND CHRISTOPHE FUMEAUX[2], (Fellow, IEEE)

[1]School of Microelectronics, Xidian University, Xi'an 710071, China
[2]School of Electrical and Electronic Engineering, The University of Adelaide, Adelaide, SA 5005, Australia

Corresponding author: Zhibin Zeng (zbzeng@163.com)

This work was supported in part by the Fundamental Research Funds for the Central Universities of China, under Grant K5051125007.

ABSTRACT A wideband common-mode (CM) suppression reconfigurable filter is proposed for high-speed all-pass differential circuits. The filter adopts three varactor-loaded compact defected ground structures (DGSs) to achieve continuous reconfigurability in its operation frequency with a large CM suppression dynamic range in the bandwidth. The varactors play an important role in widening the accessible instantaneous bandwidth and miniaturizing the structure. The three DGS cells with a total area of 15 mm x 10 mm are implemented symmetrically under the differential lines, to obtain reconfigurable CM bandstop characteristics which can be continuously adjusted from 1.8 to 8.1 GHz. A coupled LC resonator equivalent model is developed to represent and analyze the proposed filter, which explains its operation principle and assists in accelerating the reconfiguration design method. A good agreement between full-wave simulations and measured results is demonstrated, which validates the proposed design.

INDEX TERMS Reconfigurable filter, defected ground structures, common-mode suppression, varactor diode.

I. INTRODUCTION

Differential circuits have been widely used in high-speed printed-circuit board (PCB) design, since they exhibit superior signal-to-noise performance and high electromagnetic immunity against conducted and radiated interfering signals [1], [2]. However, these circuits have unavoidable imbalances in their differential mode (DM) which might generate common-mode (CM) currents. This often leads to severe electromagnetic interference (EMI) problems and unwanted electromagnetic (EM) radiation issues [3]–[6].

Various types of filters can be used to suppress CM noise. For instance, balanced bandpass filters [6]–[9] have advantage of CM-suppression in their operational frequency band. They however cannot be applied to high-speed differential digital circuits which need all-pass characteristics for differential signals. CM filters with high permeability ferrite cores [10] have been proposed to suppress the CM noise in a wide frequency range for all-pass differential signals, but they are limited in terms of their highest frequency of operation. For operation at gigahertz frequencies, multilayer low-temperature co-fired ceramic (LTCC) technology [11] provides an alternative solution. However, such multilayer designs introduce additional structure complexity and hence increase the cost of the circuit and may cause additional undesirable attenuation to the differential signal. Recently, CM filters based on complementary split ring resonators (CCSR) [12], [13], twin-ring resonator (TRR) [14], multimode slotline resonator [15], electromagnetic bandgap (EBG) structures [16], [17] and defected ground structure (DGS) [18]–[24] have been reported as new approaches. Filters proposed in [12], [14], and [15] have excellent all-stop or bandstop CM suppression, while they only operate in a given fixed frequency band. EBG-based filters can operate in all-pass band for their differential signals. However, they are not very suitable for embedded systems because of their large space requirement intrinsic to the designs. In contrast, filters employing DGS can possess simpler and more compact structure with a wideband CM suppression. Because of the limited space in high-speed

The associate editor coordinating the review of this manuscript and approving it for publication was Yuhao Liu.

PCB designs, miniaturization and bandwidth enhancement for DGS filters are essential. For instance, filters adopting periodic DGS [18]–[20] have been demonstrated to broaden the bandwidth at the cost of a larger device geometry. Filters utilizing composite DGS [1], [2] have been also shown to increase the bandwidth, by controlling the mutual coupling between various DGS patterns. A filter utilizing C-shaped DGS with meandered differential pairs has been demonstrated with a wideband CM suppression [25]. However, it adopts a relatively complex multilayered PCB and exhibits a relatively high insertion loss of around 3 dB at higher frequencies. In addition, similar filters can be found in antenna designs, aiming for CM noise rejection [21], [26]. It is worth mentioning that these aforementioned DGS-based filters have a fixed operational bandwidth, and thus can only serve for pre-defined frequency bands. By contrast, filters with reconfigurability in the operation frequency range are attracting more and more attention, because they can fulfill the requirements for dynamic spectrum access and cognitive radio.

The requirements on all-pass differential circuits [25] make it difficult to design a full-band CM filter. On the one hand, the size of a full-band CM filter will be very large, since it needs a number of band filtering cells to achieve the wide-band performance. On the other hand, the signal to noise ratio of the differential circuit will be degraded, because it is challenging to achieve a CM noise suppression capability below 15-dB over the whole band. Additionally, since CM noise originates from practical circuits and depends on the application environment [27], their characteristics such as frequency range might change when the operating conditions vary. Therefore, the development of reconfigurable CM filters to significantly increase the flexibility of the circuit applications is highly desired. Reconfigurable DGS-based devices can be implemented using PIN diodes and/or varactors. As typical examples using PIN diodes, El-Shaarawy et al. [24] proposed a reconfigurable DGS resonator on coplanar waveguide, which resulted in discretely tunable resonance frequencies from 1 to 11 GHz. Similarly, Fakharian et al. [28] proposed a reconfigurable slot antenna using four PIN diodes in meander-slot DGSs, which could switch between different discrete operation frequencies from 1.5 to 2.7 GHz. To allow continuously tunable stopband characteristics, varactors can be utilized as the tuning components instead of PIN diodes. On top of that, the use of varactors provides a method for filter miniaturization, since the variable capacitance introduced by varactors can be much larger than the equivalent capacitance of the DGS. For example, Chen et al. [23] applied a varactor-loaded slot-ring resonator in a CM suppression filter, and obtained a stopband frequency continuously tunable from 0.78 to 1.52 GHz. Dai and Li [29] proposed a CM suppression filter adopting varactor-loaded slotted ground, which had a wideband continuous tunability range from 0.80 to 2.10 GHz. In that work, the varactors were located between the pair of differential lines on the same metallization level, which increase the inter-line distance and may increase the radiated EMI of the differential line.

In this paper, a concept of wideband reconfigurable filter based on varactor-loaded DGSs is proposed, together with its equivalent circuit developed for reconfiguration analysis and design purpose. As a demonstration, a CM-suppression filter with all-pass differential signal characteristics is designed based on three varactor-loaded DGS cells. The proposed filter exhibits a wide reconfigurable CM stopband which can be tuned to cover a range extending approximately from 1.8 to 8.1 GHz, leading to a fractional tuning range of around 80.9%. The filter enables a wideband and efficient suppression of the CM noise while still maintaining a good signal quality for the differential components. The proposed design has been experimentally validated and the good agreement between simulations and measurements validates the concept.

II. WIDEBAND CONTINUOUSLY RECONFIGURABLE FILTERS

This section presents the design process of the proposed reconfigurable filter in three main steps. Firstly, a passive filter design based on the chosen DGS cells is analyzed using a simplified coupled parallel LC equivalent circuit model, illustrating the working principle of the DGS cells. Using the simplified equivalent circuit that represents key filter features is sufficient and practical to promptly describe the filter performance. It will be challenging to obtain the exact performance of the filter, through a comprehensive equivalent circuit model which considers all the filter factors such as the shape, size, location of DGS, and the characteristics of PCB materials. Secondly, a concept of reconfigurable design built on the basis of this passive filter is proposed, whose reconfigurability is achieved by loading a varactor in each DGS cell. The concept is validated through simulations based on equivalent circuit model as well as full-wave method. Thirdly, as the most critical step to realize the reconfigurable filter, the bias circuit design and a practical implementation are proposed and analyzed using a dedicated equivalent circuit model.

It is worth emphasizing that the equivalent circuit model plays two main roles in the filter design in this work. It firstly explains the DGSs basic working principle and secondly provides the circuit model basis for the reconfigurable filter design. To this end, the equivalent circuit model of a reconfigurable filter can be conveniently formed with addition of the varactor circuit model into the LC equivalent circuit model developed for the passive DGS-based filter. The new circuit model can reasonably predict the filter characteristics in a quick manner, which significantly accelerates the reconfigurable filter design. This method is efficient for designing reconfigurable filters, which will be confirmed by the good agreement between the measurements and simulations in both ANSYS HFSS and ADS. Additionally, it also suggests that the extracted LC parameters are reasonable, because of the matched simulation results in HFSS and ADS.

A. PASSIVE DGS DESIGN

Figure 1 shows the configuration and dimensions of a passive wideband CM-suppression filter. The filter consists of a pair of coplanar differential lines and a ground plane where a series of DGS cells are etched. These DGSs include two C-shaped and one H-shaped structures which are kept symmetrical with respect to the coplanar differential lines. This arrangement is critical as it does not significantly affect the differential signals, since these signals are transmitted in the odd mode and their return currents on the ground plane are relatively weak [3]. In contrast, the CM signal propagation strongly relies on the currents in the ground plane. Therefore, the CM-suppression characteristic of this type of filters is attained because the DGS structures alter the ground plane current distribution. Hence the CM-suppression band is mainly determined by the patterns and dimensions of the DGSs. Sensitivity of the filter performance to the DGS dimensions was investigated in [30], noting that similar conclusions are found directly applicable to our filters and are therefore not repeated for the sake of brevity.

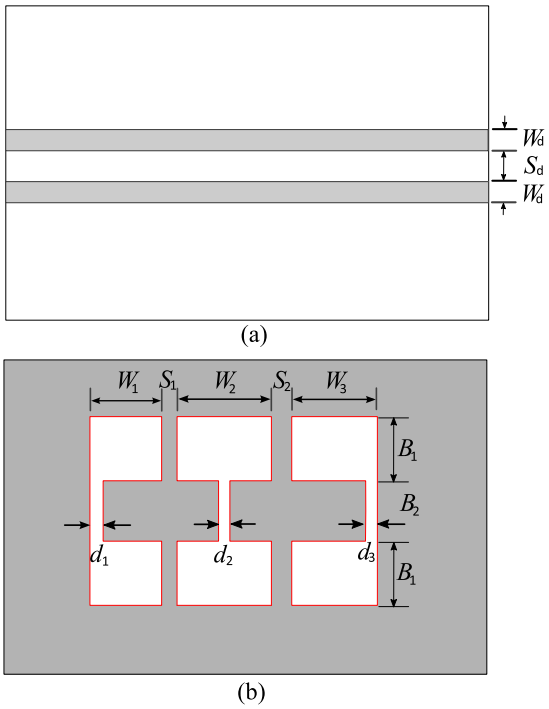

FIGURE 1. Configuration of the proposed passive DGS-based CM filter, (a) top view showing the pair of coplanar differential lines, and (b) bottom view showing the DGS structures. Dimensions (mm): $W_1 = 3.8$, $W_2 = 5$, $W_3 = 4.5$, $S_1 = 0.7$, $S_2 = 1$, $d_1 = d_3 = 0.7$, $d_2 = 0.6$, $W_d = 0.9$, $S_d = 0.8$, $B_1 = 3.4$, $B_2 = 3.2$.

The simplified equivalent circuit model of the filter shown in Fig. 1 is depicted in Fig. 2. The differential lines above the DGS are modelled as an ideal transmission line with even-mode characteristic impedance Z, and a parallel LC resonator is utilized to represent each DGS cell cascaded on the ground plane [1]. Since the DGS patterns is symmetric, the even-mode equivalent circuit model analysis of the proposed filter can be based on a two-port equivalent-circuit model for simplification, which is explained in detail

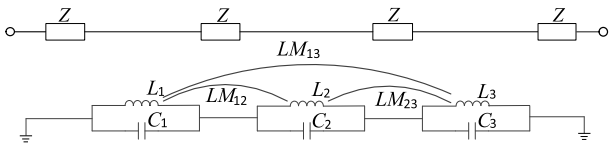

FIGURE 2. Equivalent LC resonant circuit model for the proposed passive DGS-based filter in its CM mode.

in [1], [3], [19], [30], and [31]. These three parallel LC resonators block the unwanted CM noise at their resonance frequency. The variable $C_i (i = 1, 2, 3)$ denotes the resonator's capacitance which is formed between two sides of the narrow slit in the DGS, while $L_i (i = 1, 2, 3)$ indicates the inductance which is formed along the DGS edges. There exist mutual inductances and capacitances between the DGS cells. However, since the distances between adjacent central gaps are far longer than the distances between adjacent metal traces in the center of the DGS cells, the coupling coefficients associated with the equivalent mutual capacitances are much smaller than that of mutual inductances. Additionally, the values of mutual capacitances are much smaller than the typical capacitance of the varactor. Therefore, for ease of understanding and analysis, only mutual inductances $LM_{ij} (ij = 12, 13, 23)$ between adjacent DGS cells are considered here. These mutual inductances are beneficial for the filter performance, as they widen the stopband for CM noise. As these variables are the most dominant parameters of the DGSs, the proposed simplified circuit model can efficiently represent and analyze the filter performance.

The equivalent parameters of each DGS cell can be derived from full-wave simulations (performed with HFSS) [1], [30], [32], [33]. The impedance $Z_i (i = 1, 2, 3)$ of the resonators can be denoted as

$$Z_i = \frac{j\omega L_i}{1 - \omega^2 L_i C_i}, \tag{1}$$

The CM transmission coefficient S_{21} can be written as

$$S_{21} = \frac{2Z}{2Z + Z_i}, \tag{2}$$

where Z is the even-mode characteristic impedance of the coupled differential pairs. According to the definition of the lower 3 dB cutoff frequency ω_{ci} $(i = 1, 2, 3)$, we get

$$|S_{21}(\omega_{ci})|^2 = \left|\frac{2Z}{2Z + Z_i}\right|^2 = \frac{1}{2}. \tag{3}$$

Substituting Equation (1) into Equation (3) to remove Z_i, Z can be rewritten as

$$Z = \frac{\omega_{ci} L_i}{2(1 - \omega_{ci}^2 L_i C_i)}. \tag{4}$$

As the resonance angular frequency ω_{oi} $(i = 1, 2, 3)$ of the LC resonator can be expressed as

$$\omega_{oi} = \frac{1}{\sqrt{L_i C_i}}, \tag{5}$$

C_i and L_i can be determined from ω_{ci} and ω_{oi}. Substituting Equation (5) for L_iC_i into Equation (2), then L_i and C_i (i = 1, 2, 3) are extracted as follows:

$$L_i = \frac{2Z}{\omega_{ci}} \frac{\omega_{oi}^2 - \omega_{ci}^2}{\omega_{oi}^2}$$
$$C_i = \frac{1}{2Z} \frac{\omega_{ci}}{\omega_{oi}^2 - \omega_{ci}^2}. \quad (6)$$

For the mutual inductance, the parameters can be estimated according to [34]

$$LM_{ij} = -0.5\sqrt{L_iL_j}\left(\frac{f_{oi}}{f_{oj}} + \frac{f_{oj}}{f_{oi}}\right) \times \sqrt{\left(\frac{f_i^2 - f_j^2}{f_i^2 + f_j^2}\right)^2 - \left(\frac{f_{oi}^2 - f_{oj}^2}{f_{oi}^2 + f_{oj}^2}\right)^2}, \quad (7)$$

where f_{oi} and $f_{oj}(f_{oi} > f_{oj})$ denotes respectively the self resonance frequency (i.e., in absence of coupling) of the two considered DGS units, while f_i and $f_j(f_i > f_j)$ stand for their two split resonance frequencies because of the coupling [1].

The simulated CM transmission coefficients ($|S_{cc}21|$) of each of the three DGS cells in HFSS are shown in Fig. 3, from where the lower 3 dB cutoff angular frequency ω_{ci} as well as resonance angular frequencies ω_{oi} are obtained. The calculated equivalent capacitance and inductance of each DGS are shown in Table 1, together with the mutual inductances between them.

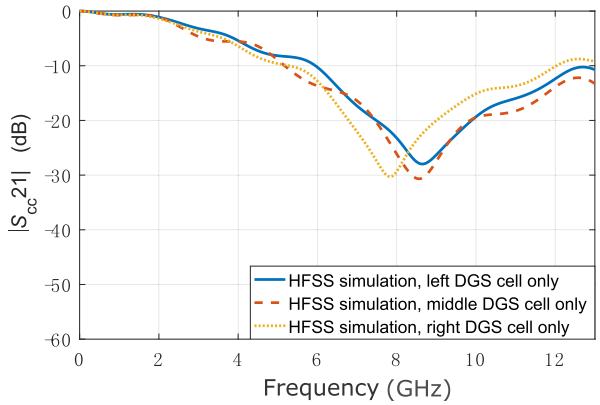

FIGURE 3. Simulated $|S_{cc}21|$ of the filter with each DGS cell considered individually in HFSS simulation.

TABLE 1. LC equivalent circuit values for each DGS cell and their mutual inductance in CM operation.

Parameters	L_1	L_2	L_3
Value (nH)	5.48	6.44	5.79
Parameters	C_1	C_2	C_3
Value (pF)	0.065	0.058	0.076
Parameters	L_{M12}	L_{M23}	L_{M13}
Value (nH)	-0.80	-0.66	-0.10

The simulated $|S_{cc}21|$ parameters based on HFSS and the corresponding results from the equivalent circuit model simulated using Advanced Design System 2011 (ADS) are depicted in Fig. 4, where a satisfactory agreement is observed. The HFSS results indicate that the filter has a wide 15-dB CM stopband from 3.7 to 13.0 GHz, whereas a similar range between 3.5 to 12.5 GHz is observed from the equivalent circuit model. The small discrepancy is caused by the simplified equivalent circuit model, which does not consider all distributed effects. Nevertheless, this equivalent circuit model is accurate enough to analyze the performance of this passive filter.

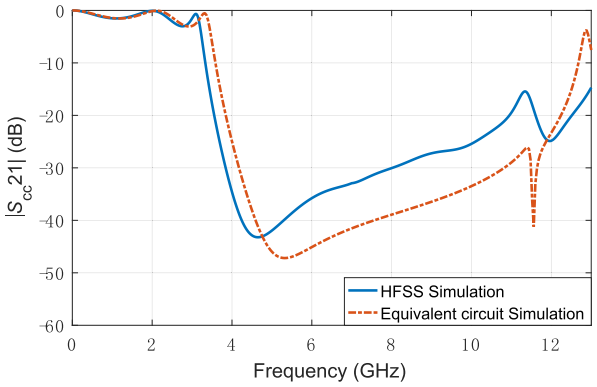

FIGURE 4. Simulated $|S_{cc}21|$ of the filter from full-wave simulation and equivalent circuit modeling.

B. RECONFIGURABLE DGS DESIGN

In order to endow the passive filter with continuous reconfigurability in its operation frequency, varactors are adopted as a tunable capacitor in conjunction with the DGS cells. The varactor capacitance has a significant influence on the filter performance because it is much larger than the equivalent capacitance of a DGS cell. A larger capacitance theoretically leads to a lower operation frequency. Considering the path of the return CM currents, it is found that the best location to load a varactor is in the middle of the DGS cell. This corresponds to the shortest path of the return CM currents and maximizes the effect of a single varactor while preserving a symmetric circuit design, as shown in Fig. 5. It is emphasized that the ideal varactor connection illustrated in Fig. 5 is only for preliminary design and analysis, where the corresponding bias network is not considered. A commercially available varactor MA46H120 (MACOM Technical Solutions) is chosen for the design as it provides a large capacitance tuning ratio of around 1:10 and a small internal resistance of 2 Ω approximately [35]. Compared to the minimum achievable capacitance (in the order of 0.12 pF) of MA46H120, the equivalent capacitance of the DGS cells, as indicated in Table 1, is small. Therefore, by introducing varactors into their DGS structure(s), the filters can significantly lower their resonance frequency. This can be observed in Fig. 6, where the HFSS simulated CM transmission coefficients is displayed for a filter with a single DGS cell

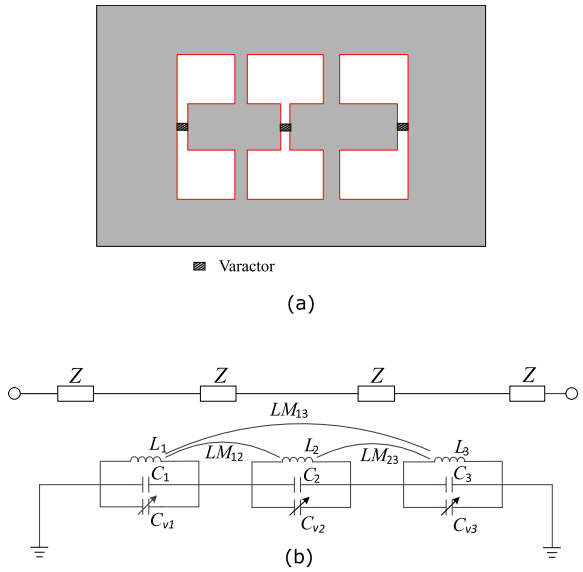

FIGURE 5. Schematic diagram of the ideal reconfigurable DGS-based CM filter (i.e., without bias circuit) with varactor-loaded DGS: (a) bottom view, and (b) equivalent LC resonant circuit model for the CM.

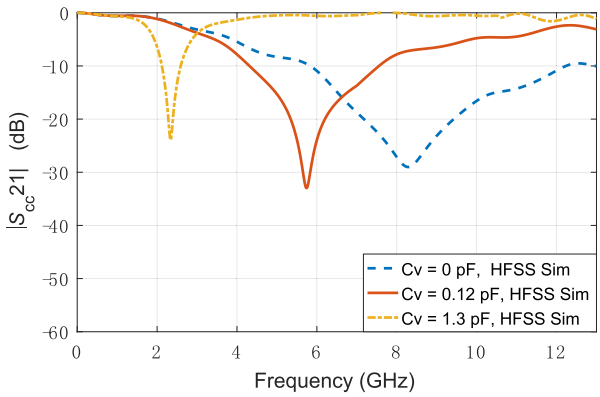

FIGURE 6. Simulated $|S_{cc}21|$ of a filter including only the left DGS cell loaded with a varactor with capacitance of 0.12 or 1.3 pF, compared to corresponding simulation without varactor (i.e., 0 pF).

(the left one), which is loaded with a varactor with various capacitances. When the MA46H120 varactor exhibits its minimum achievable capacitance of 0.12 pF and the maximum value of 1.3 pF, the DGS resonance frequency significantly decreases compared to the case without a varactor, as governed by Equation (5).

The same observation can be extended to the 3-element reconfigurable CM filter. This is illustrated in Fig. 7 where the simulated CM transmission coefficients of the filter shown in Fig. 5 are displayed for three cases, namely the original static case without varactor and the tunable cases with equal values of varactor capacitances $C_{v1} = C_{v2} = C_{v3}$ set to the available extreme values. It is observed that the 15-dB CM bandstop frequency range shifts from a band of 3.7 - 12.6 GHz in the unloaded case, to a band of 3.0 - 9.2 GHz for the minimal value of capacitance of 0.12 pF. It then decreases further to a band of 1.8 - 3.6 GHz

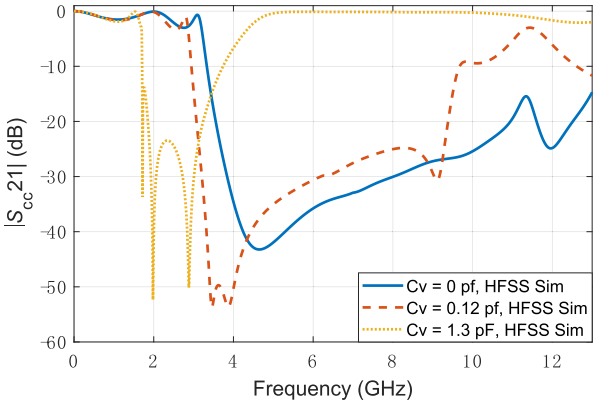

FIGURE 7. Simulated $|S_{cc}21|$ of the filter shown in Fig. 5, loaded with varactor capacitance set to 0 (i.e., no varactor), 0.12 and 1.3 pF respectively.

for the maximal value of capacitance of 1.3 pF. It is also observed that the fractional bandwidth of the stopband decreases from more than 109% for the minimal varactor capacitance, to 67% for the largest varactor capacitance value, as expected due to the device miniaturization.

To characterize the filter sensitivity to the varactor capacitance, a HFSS-based study has been conducted and the results are shown in Fig. 8. The figure shows the lower and upper cut-off frequencies of the filter operation band versus (hypothetical) varactor capacitance varying over several orders of magnitude, namely from 0.01 to 10 pF, with a grey area highlighting the chosen (practical) varactors capacitance range. One can observe that the higher values of varactor capacitance lead to lower cut-off frequencies, i.e., a more miniaturized filter, however at the cost of a narrower relative bandwidth. As indicated by the shaded area in Fig. 8, the chosen varactor provides a relatively wide bandwidth change) which can be beneficial for applications that require a larger dynamic range in the bandwidth.

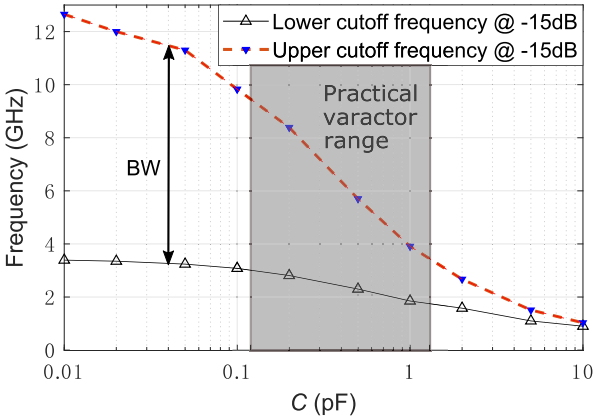

FIGURE 8. Upper cutoff frequency and Lower cutoff frequency for different varactor capacitance C. The shaded part show the capacitance range of the chosen varactor, i.e., $[C_{min}, C_{max}] = [0.12, 1.30]$ pF.

The simulated DM transmission coefficients of the proposed filter loaded with three different typical varactor capacitances of 0 (no varactor), 0.12 (minimum value of the

chosen varactor) and 1.3 pF (maximum value) are shown in Fig. 9. It can be seen that these three $|S_{dd}21|$ parameters are very close to 0 dB and no less than −0.3 dB in the frequency range from 0 to 8.1 GHz, which is indicative of a small DM transmission loss. Furthermore, the $|S_{dd}21|$ result when the filter does not have any DGS (ideal ground) is also shown in the figure, where a very slight discrepancy from the three curves is found in the range from DC to 9 GHz. These results suggest that the DM transmission characteristic impedance is nearly unaffected by the DGS cells and thus the DM performance is satisfactory from 0 to 8.1 GHz. However, when the frequency increases beyond 10 GHz, i.e., beyond the claimed range of operation, the DM transmission performance deteriorates significantly, since the DGS cells become effectively larger and hence start to exhibit a prominent effect on the DM characteristic impedance.

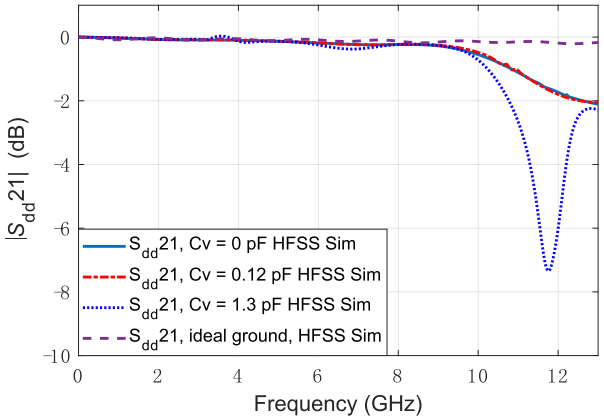

FIGURE 9. Simulated $|S_{dd}21|$ of the differential microstrip line when there is the DGS filter loaded with varactor capacitance set to 0 (i.e., no varactor), 0.12 and 1.3 pF respectively, and there is perfect ground.

C. PRACTICAL IMPLEMENTATION OF THE RECONFIGURABLE FILTER

Based on the investigations shown in the previous section, varactor-loaded DGSs have been shown to be a promising solution to design reconfigurable filters. This section considers the practical realization of this solution. One of the most critical steps in reconfigurable CM filter design is the bias circuit implementation. The bias circuit schematic for the proposed filter is depicted in Fig. 10. The varactor (C_v) across the DGS slot is connected between ground and a controllable power supply via an inductor (L) and a resistor (R) for RF isolation. In order to reduce the effect of the RF isolation branch, the resistor (R) needs to be large enough (i.e., 1 MΩ) and placed as close as possible to the pad.

When both sides of the DGS gap are connected to the DC-ground, a DC-blocking capacitance C must be used to connect the varactor diode across the gap. In general, this DC-blocking capacitance should be markedly larger than that of the varactor, so that its effect can be omitted. It is noted that this DC-blocking capacitance cannot be realized with another varactor, since two capacitors in series would lower the adjustable capacitance range.

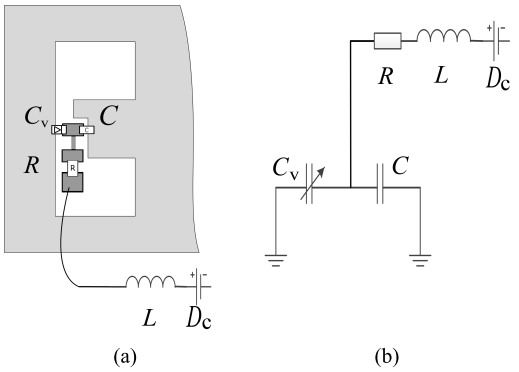

FIGURE 10. Bias circuit design for the proposed filter: (a) configuration of C_v and C in the DGS and (b) schematic of the biasing circuit, DC-blocking capacitor and varactor for the varactor diodes in the proposed filter, where L, R, C and C_v are the RF-choke inductor, RF-blocking resistor, DC-blocking capacitor and varactor, respectively.

To accommodate and connect the varactors and the DC-blocking capacitors, a small island pad is introduced in the middle gap of each DGS. The dimensions of these three pads are shown in Fig. 11. Since these island pads are small and the width of gap is increased accordingly, their influence on the filter performance is modest. The simulated CM transmission coefficients $|S_{cc}21|$ of the filters with and without the island pads are shown in Fig. 12, confirming the low impact of the island pads.

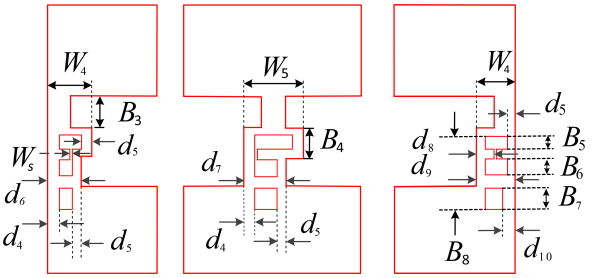

FIGURE 11. Bottom view of the implemented wideband reconfigurable DGS filter. Dimensions (mm) of modified parameters for adding varactor diodes: $B_3 = 0.9$, $B_4 = 1.4$, $B_5 = 0.8$, $B_6 = 1.0$, $B_7 = 1.2$, $B_8 = 3.4$, $d_4 = 0.2$, $d_5 = 0.3$, $d_6 = 1.4$, $d_7 = 1.3$, $d_8 = 0.9$, $d_9 = 1.8$, $d_{10} = 0.5$, $W_4 = 1.8$, $W_5 = 2.0$, $W_s = 0.2$.

In general, the equivalent circuit model of variable capacitance and DC-blocking capacitance cannot be simply treated as capacitor in RF circuits. Considering their typical characteristics, both equivalent circuits of the varactor and the DC-blocking capacitor consist of a resistor, an inductor and a capacitor in series, as shown in Fig. 13a. According to [35], the chosen varactor MA46H120 effectively has an internal resistance $R_v = 2$ Ω, an inductance $L_v = 0.05$ nH and a variable capacitance C_v ranging from 0.12 to 1.3 pF, whereas the DC-blocking capacitor equivalently shows a capacitance $C_c = 22$ nF, a resistor $R_c = 0.3$ Ω and an inductance $L_c = 0.2$ nH [36]. Because C_c is much larger than C_v, it can be in principle omitted when simplifying the equivalent circuit. The equivalent resistance R_s, capacitance C_s and inductance

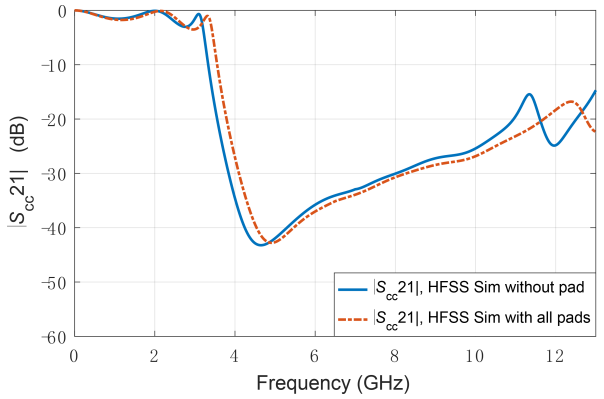

FIGURE 12. Simulated $|S_{CC}21|$ of the filter with and without the island pads required for biasing the varactors.

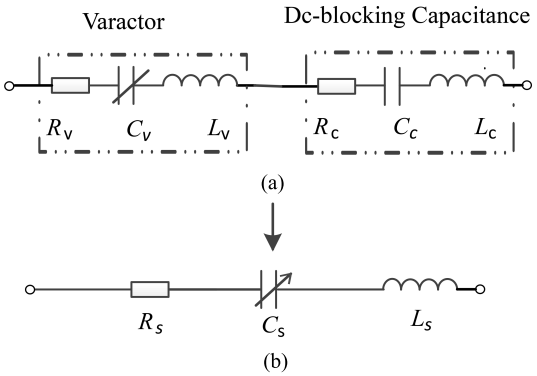

FIGURE 13. (a) The equivalent circuit of a varactor and a DC-blocking capacitor in series and (b) its simplified model.

L_s for the in-series varactor and by-pass capacitor can be obtained as follows: $R_s = R_v + R_c = 2.3\ \Omega$, $C_s = C_v$ and $L_s = L_v + L_c = 0.25$ nH, as depicted in Fig. 13b.

By replacing C_v in Fig. 5 with this series equivalent circuit, a new overall equivalent circuit is formed, as shown in Fig. 14. Because the varactor and the by-pass capacitance lie within the slot of the DGS, their equivalent circuit is in parallel with the DGS equivalent capacitor in the schematic level simulation in ADS.

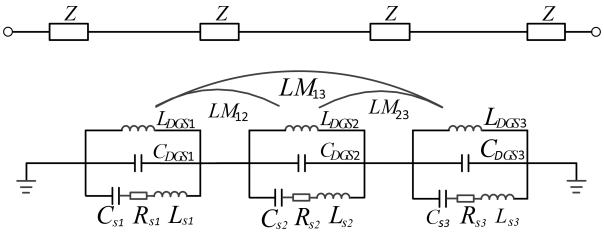

FIGURE 14. Equivalent circuit for the CM of the final reconfigurable filter.

As shown in Fig. 15, ADS simulation of this circuit model leads to results that are in good agreement with the ones obtained from HFSS for $C_v = 0.12$ pF, i.e., in the high frequency response range. However, there exists a small discrepancy in the low frequency performance, that is, the CM

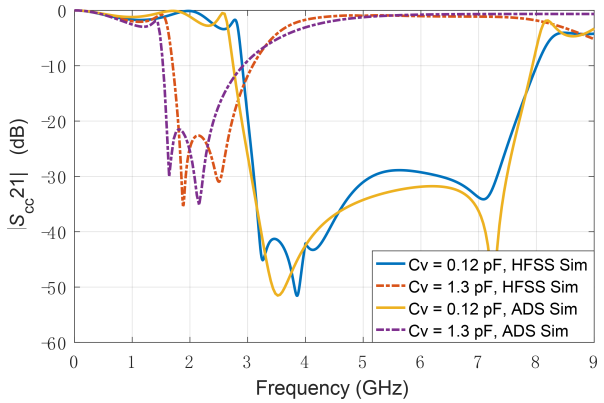

FIGURE 15. Simulated $|S_{CC}21|$ of the proposed reconfigurable filter using ADS and HFSS, when Cv = 0.12 and 1.3 pF respectively.

TABLE 2. equivalent LC parameters of each DGS cell under different varactor conditions.

LC Parameters	No Cv	Cv@0.12 pf	Cv@1.3 pf
L_{eff1} (nH)	5.48	5.23	4.56
L_{eff2} (nH)	6.44	6.2	5.71
L_{eff3} (nH)	5.79	5.78	5.3
C_{eff1} (pF)	0.065	0.186	1.21
C_{eff2} (pF)	0.058	0.176	1.12
C_{eff3} (pF)	0.076	0.190	1.15

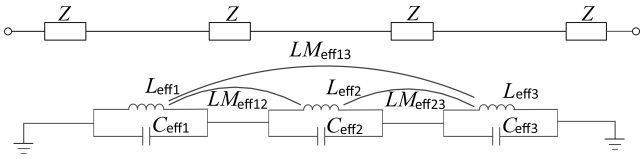

FIGURE 16. Simplified equivalent CM circuit of the final reconfigurable filter.

bandstop calculated from ADS is slightly lower than that from HFSS by around 200 MHz. The main reason is most likely the idealized assumption that the parasitic inductance and internal resistance of the varactor are constants. The assumption of constant inductance is most likely not accurate. To understand this, the circuit model shown in Fig. 14 is further simplified as an LC circuit which consists of an equivalent DGS inductor in parallel with an equivalent DGS capacitor, as shown in Fig. 16. The values of the calculated equivalent lumped components are shown in Table 2. When the varactor capacitance is increasing, the DGS equivalent capacitance $C_{effi}(i = 1, 2, 3)$ follows the trend, while the equivalent DGS inductances $L_{effi}(i = 1, 2, 3)$ are found to be decreasing, which confirms that the assumption of constant inductance is only an approximation. As a result, the resonance frequency of the filter simulated in ADS is lower than that obtained from HFSS, as governed by (5). It is also noted that the C_{effi} values are very similar to that of the varactors, because the varactor capacitance is dominant in the circuit.

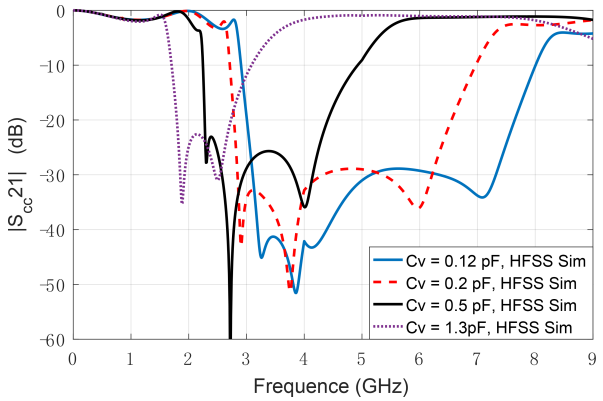

FIGURE 17. Full-wave simulated $|S_{cc}21|$ of the proposed reconfigurable filter when $C_{v1} = C_{v2} = C_{v3} = 0.12$, 0.2, 0.5 and 1.3 pF respectively.

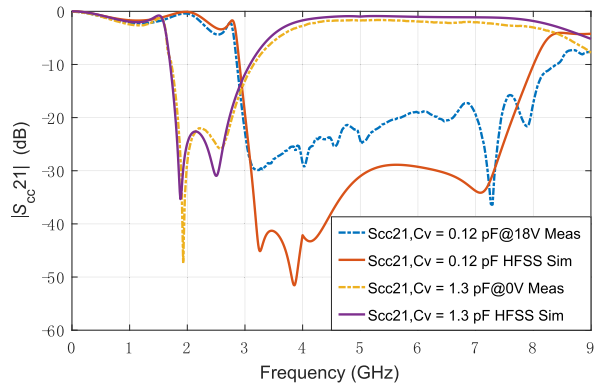

FIGURE 18. Simulated and measured CM transmission coefficients of the proposed reconfigurable filter.

D. BIASING VOLTAGE CONFIGURATION

This section investigates whether the use of more than one power supply to individually bias the three varactors is required for seamless coverage of a large range of frequencies. Figure 17 shows the full-wave simulated CM transmission coefficients of the proposed reconfigurable filter for the case where all the varactors are controlled by one power supply. According to these results, it is observed that the filter is able to provide a minimum CM-suppression level of 15 dB over its operating frequency range, when all the varactors are of the same capacitance. This implies that, with only one power supply to bias the three varactors, the filter is readily able to provide a satisfactory tunable CM suppression performance.

III. EXPERIMENTAL RESULTS

To validate the proposed filter design, a prototype has been fabricated on a 381-μm thick Rogers TMM3 substrate with a relative permittivity of 3.27 and a loss tangent of 0.002. The overall dimensions of the PCB for the filter are 65×45 mm^2. The fabricated filter with the bias circuit integrated is illustrated in Fig. 19. The filter prototype is measured using a vector network analyzer N5230A.

Comparison between the simulated and measured $|S_{cc}21|$ results is shown in Fig. 18. The simulated CM suppression

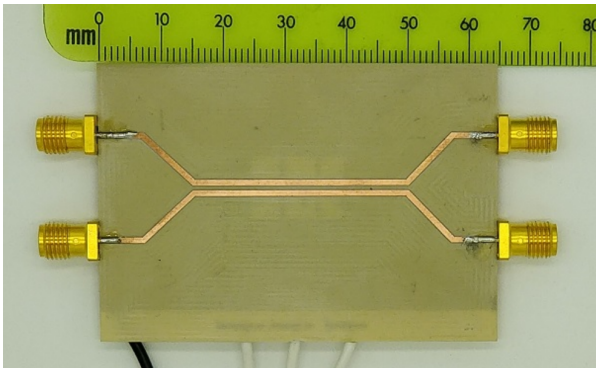

(a)

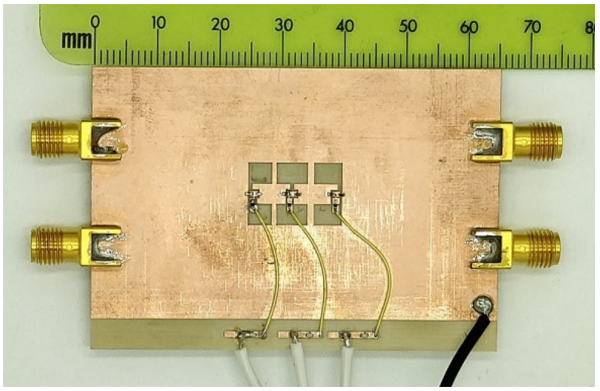

(b)

FIGURE 19. The reconfigurable CM-suppression filter prototype: a) top view and b) bottom view.

range (defined for a CM transmission coefficient less than -15 dB) extends from 1.8 to 2.9 GHz centered at 2.35 GHz when all $C_v = 1.3$ pF. This range can be continuously tuned to reach 3.0 to 7.8 GHz centered at 5.4 GHz when all $C_v = 0.12$ pF. This compares favorably with the measured results, where the same range is obtained for the highest capacitance and a slightly shifted range of 3.0 to 8.1 GHz was predicted for the lowest capacitance. The measurements generally agree well with the simulations at the lower frequency range, while in the higher frequency range, the measured results exhibit a lower signal attenuation level and a slightly wider stop band. Overall, a good agreement between HFSS simulation and measurement is attained. The discrepancy between them can be mainly explained by the following reasons. First, the lumped RLC parameters of the varactor and the DC blocking capacitor are set constant in HFSS, however these values are frequency-dependent and can change in a small range. Second, in order to facilitate testing with SMA connectors, the gap between the differential lines needs to be increased at the two terminals (as visible in Fig. 19). This arrangement leads to a slightly increased DM impedance and a slightly decreased CM impedance and thus small variations in the impedance matching of the whole circuit. Third, the parasitic capacitances formed between the soldered lumped components and the ground are not considered in the simulations. Finally, the imperfect materials and fabrication tolerances also introduce the discrepancies. Overall, as shown

TABLE 3. comparison among various reconfigurable filters.

Ref	Ref [23]	Ref [24]	Ref [29]	Ref [37]	Ref [38]	Ref [31]	this work
Filter type	common-mode	bandstop	common-mode	bandstop	bandstop	bandpass	common-mode
Permittivity	3.38	9.5	2.65	4.6	3.48	6.03	3.27
Size (λ_g)	0.59×0.11	0.26×1.32	0.39×0.41	0.23×0.73	0.096×0.21	0.078×0.16	0.36×0.24
Active component	0.57-6.6 pF	PIN	0.75-15 pF	0.4-2.5 pF	0.54-6.6 pF	2.0-4.5 pF	0.12-1.3 pF
Tuning type	Continuous	Discrete	Continuous	Continuous	Continuous	Continuous	Continuous
Center frequency range (GHz)	0.78-1.52	1.5-7.5	0.8-2.1	3.7-7.4	1.69-2.16	0.64-0.93	2.35-5.4
Tuning range (GHz)	0.72-1.63	N/A	0.75-2.63	3.4-4.5, 6-8.5	1.6-2.3	0.6-0.96	1.8-8.1
Fractional Tuning range	64.3%	N/A	89.7%	19%	24.4%	36.9%	78.7%
BW_{min} (GHz)	0.14	0.3	0.24	0.70	0.2	0.06	1.1
BW_{max} (GHz)	0.3	0.8	1.1	1.4	0.43	0.08	4.8
$FractionalBW_{min}$	14%	32%	28%	—	12%	9%	50%
$FractionalBW_{max}$	20%	11%	53%	—	27%	8.7%	84%
Maximum loss of signal (dB)	1.2	—	1.2	4	—	2	1.4

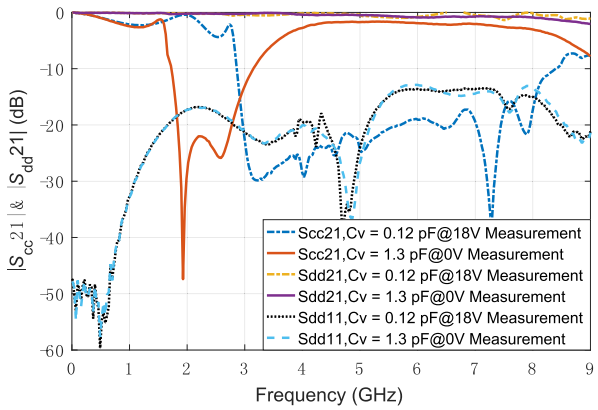

FIGURE 20. Measured DM transmission and reflection coefficients for the proposed reconfigurable filter with bias voltage of 0 and 18 V respectively.

in Fig. 18, the achievable tuning range covers 1.8 to 8.1 GHz.

In addition, the measured DM transmission coefficients $|S_{dd}21|$ are also shown in Fig. 20, where a very small insertion loss is observed from simulations. That is, when $C_{v2} = 1.3$ pF, the measured $|S_{dd}21|$ parameter remains above -1 dB over the whole operation band, and when $C_{v2} = 0.12$ pF, it has a drop capped at -1.4 dB in a narrow bandwidth between 7.2 to 7.4 GHz. The measured $|S_{dd}11|$ is below -10-dB within the frequency range from 0 to 8.1 GHz. These results imply that the filter performance in the DM is insensitive to the bias status. This can be understood considering that, since the differential signals propagate in the odd mode, the currents returning through the ground plane are negligible.

A comparison between the proposed reconfigurable CM-suppression filter and recently reported differential tunable filters adopting DGS cells is summarized in Table 3. Since there exist only a few reports about the design of reconfigurable CM filters, we extend the comparison table to include filters with other functionalities, i.e., reconfigurable band-stop filters and a reconfigurable band-pass filter. While direct comparison is not appropriate, the collected data is illustrative of achievable performances in various configurations. The minimum and maximum bandwidths of the proposed filter are 1.1 and 4.8 GHz respectively, which is more than that of the other filters. Furthermore, the fractional bandwidth of the proposed filter is 78.7%, which is only slightly less than that in [29], however, the area of the latter is about twice the area of the proposed filter. Compared with [23] and [29] which are other reported reconfigurable CM filter, the proposed filter has a wider bandwidth for CM noise suppression.

IV. CONCLUSION

A continuously reconfigurable DGS-based CM-suppression filter adopting varactors has been presented. Simplified equivalent circuit models for the presented passive and reconfigurable filters have been developed and utilized for prompt filter design and analysis. By changing the bias voltage to the varactors, the frequency range (defined by the CM transmission coefficient being less than -15 dB) of the proposed filter is measured to be continuously tunable from a range of 1.8 - 2.9 GHz to a range of 2.9 - 8.1 GHz. This leads to an effective tuning range from 1.8 to 8.1 GHz. Additionally, the DM transmission coefficient $|S_{dd}21|$ is mainly less than -1 dB, offering excellent DM performance which is an essential requirement for CM-suppression filters. To the authors' best knowledge, this filter exhibits the largest tuning range and widest bandwidth in the stop band, among the reported CM-suppression filters in the open literature. All these findings indicate that the proposed reconfigurable filters based on varactor-loaded DGS is promising for a wide range of devices in high speed digital design and microwave devices.

REFERENCES

[1] S.-J. Wu, C.-H. Tsai, T.-L. Wu, and T. Itoh, "A novel wideband common-mode suppression filter for gigahertz differential signals using coupled patterned ground structure," *IEEE Trans. Microw. Theory Techn.*, vol. 57, no. 4, pp. 848–855, Apr. 2009.

[2] Z. Zeng, Y. Yao, and Y. Zhuang, "A wideband common-mode suppression filter with compact-defected ground structure pattern," *IEEE Trans. Electromagn. Compat.*, vol. 57, no. 5, pp. 1277–1280, Oct. 2015.
[3] F. Martín *et al.*, "The beauty of symmetry: Common-mode rejection filters for high-speed interconnects and band microwave circuits," *IEEE Microw. Mag.*, vol. 18, no. 1, pp. 42–55, Jan./Feb. 2017.
[4] G.-H. Shiue, C.-M. Hsu, C.-L. Lou, and C.-F. Su, "A comprehensive investigation of a common-mode filter for gigahertz differential signals using quarter-wavelength resonators," *IEEE Trans. Compon., Packag., Manuf. Technol.*, vol. 4, no. 1, pp. 134–144, Jan. 2014.
[5] F. de Paulis, L. Raimondo, S. Connor, B. Archambeault, and A. Orlandi, "Compact configuration for common mode filter design based on planar electromagnetic bandgap structures," *IEEE Trans. Electromagn. Compat.*, vol. 54, no. 3, pp. 646–654, Jun. 2012.
[6] L.-H. Zhou, Y.-L. Ma, J. Shi, J.-X. Chen, and W. Q. Che, "Differential dual-band bandpass filter with tunable lower band using embedded DGS unit for common-mode suppression," *IEEE Trans. Microw. Theory Techn.*, vol. 64, no. 12, pp. 4183–4191, Dec. 2016.
[7] P. Li, H. Chu, D. Zhao, and R.-S. Chen, "Compact dual-band balanced SIW bandpass filter with improved common-mode suppression," *IEEE Microw. Wireless Compon. Lett.*, vol. 27, no. 4, pp. 347–349, Apr. 2017.
[8] W. Feng, W. Che, and Q. Xue, "Balanced filters with wideband common mode suppression using dual-mode ring resonators," *IEEE Trans. Circuits Syst. I, Reg. Papers*, vol. 62, no. 6, pp. 1499–1507, Jun. 2015.
[9] Y. C. Li and Q. Xue, "Tunable balanced bandpass filter with constant bandwidth and high common-mode suppression," *IEEE Trans. Microw. Theory Techn.*, vol. 59, no. 10, pp. 2452–2460, Oct. 2011.
[10] K. Yanagisawa, F. Zhang, T. Sato, K. Yamasawa, and Y. Miura, "A new wideband common-mode noise filter consisting of Mn-Zn ferrite core and copper/polyimide tape wound coil," *IEEE Trans. Magn.*, vol. 41, no. 10, pp. 3571–3573, Oct. 2005.
[11] B.-C. Tseng and L.-K. Wu, "Design of miniaturized common-mode filter by multilayer low-temperature co-fired ceramic," *IEEE Trans. Electromagn. Compat.*, vol. 46, no. 4, pp. 571–579, Nov. 2004.
[12] H. Wang *et al.*, "Analysis of coupled cross-shaped resonator and its application to differential bandpass filters design," *IEEE Trans. Microw. Theory Techn.*, vol. 62, no. 12, pp. 2942–2953, Dec. 2014.
[13] G. Chaudhary, Y. Jeong, and J. Lim, "Harmonic suppressed dual-band bandpass filters with tunable passbands," *IEEE Trans. Microw. Theory Techn.*, vol. 60, no. 7, pp. 2115–2123, Jul. 2012.
[14] L.-H. Zhou and J.-X. Chen, "Differential dual-band filters with flexible frequency ratio using asymmetrical shunt branches for wideband CM suppression," *IEEE Trans. Microw. Theory Techn.*, vol. 65, no. 11, pp. 4606–4615, Nov. 2017.
[15] X. Guo, L. Zhu, K.-W. Tam, and W. Wu, "Wideband differential bandpass filters on multimode slotline resonator with intrinsic common-mode rejection," *IEEE Trans. Microw. Theory Techn.*, vol. 63, no. 5, pp. 1587–1594, May 2015.
[16] F. De Paulis, M. Cracraft, C. Olivieri, S. Connor, A. Orlandi, and B. Archambeault, "EBG-Based common-mode stripline filters: Experimental investigation on interlayer crosstalk," *IEEE Trans. Electromagn. Compat.*, vol. 57, no. 6, pp. 1416–1424, Jul. 2015.
[17] Q. Liu *et al.*, "Reduction of EMI due to common-mode currents using a surface-mount EBG-based filter," *IEEE Trans. Electromagn. Compat.*, vol. 58, no. 5, pp. 1440–1447, Oct. 2016.
[18] M. Kim, "Periodically corrugated reference planes for common-mode noise suppression in high-speed differential signals," *IEEE Trans. Electromagn. Compat.*, vol. 58, no. 2, pp. 619–622, Apr. 2016.
[19] W.-T. Liu, C.-H. Tsai, T.-W. Han, and T.-L. Wu, "An embedded common-mode suppression filter for GHz differential signals using periodic defected ground plane," *IEEE Microw. Wireless Compon. Lett.*, vol. 18, no. 4, pp. 248–250, Apr. 2008.
[20] L. Wang, Z. Xing, K. Wei, R. Xu, and J. Li, "S-shaped periodic defected ground structures to reduce microstrip antenna array mutual coupling," *Electron. Lett.*, vol. 52, no. 15, pp. 1288–1290, 2016.
[21] E. Colín-Beltrán, A. Corona-Chávez, T. Itoh, and J. E. Mendoza-Torres, "Circular aperture slot antenna with common-mode rejection filter based on defected ground structures for broad band," *IEEE Trans. Antennas Propag.*, vol. 61, no. 5, pp. 2425–2431, May 2013.
[22] C. Kumar and D. Guha, "Nature of cross-polarized radiations from probe-fed circular microstrip antennas and their suppression using different geometries of defected ground structure (DGS)," *IEEE Trans. Antennas Propag.*, vol. 60, no. 1, pp. 92–101, Jan. 2012.
[23] J.-X. Chen, W.-J. Zhou, W.-W. Yang, X.-F. Zhang, and Z.-H. Bao, "Wideband tunable common-mode suppression filter based on varactor-loaded slot-ring resonator for high-speed differential signals," *IET Microw. Antennas Propag.*, vol. 11, no. 2, pp. 151–157, Jan. 2017.
[24] H. B. El-Shaarawy, F. Cocceti, R. Plana, M. El-Said, and E. A. Hashish, "Novel reconfigurable defected ground structure resonator on coplanar waveguide," *IEEE Trans. Microw. Theory Techn.*, vol. 58, no. 11, pp. 3622–3628, Nov. 2010.
[25] T.-W. Weng, C.-H. Tai, C.-H. Chen, D.-H. Han, and T.-L. Wu, "Synthesis model and design of a common-mode bandstop filter (CM-BSF) with an all-pass characteristic for high-speed differential signals," *IEEE Trans. Microw. Theory Techn.*, vol. 62, no. 8, pp. 1647–1656, Aug. 2014.
[26] A. K. Horestani, M. Durán-Sindreu, J. Naqui, C. Fumeaux, and F. Martin, "S-shaped complementary split ring resonators and their application to compact differential bandpass filters with common-mode suppression," *IEEE Microw. Wireless Compon. Lett.*, vol. 24, no. 3, pp. 149–151, Mar. 2014.
[27] R. Lee Ozenbaugh and T. M. Pullen, *EMI Filter Design*, 3rd ed. Boca Raton, FL, USA: CRC Press, 2011.
[28] M. M. Fakharian, P. Rezaei, and A. A. Orouji, "A novel slot antenna with reconfigurable meander-slot DGS for cognitive radio applications," *Appl. Comput. Electromagn. Soc. J.*, vol. 30, no. 7, pp. 748–753, 2015.
[29] H.-Y. Dai and L. Li, "Wideband tunable high common-mode suppression filter based on varactor-loaded slotted ground," *Prog. Electromagn. Res. Lett.*, vol. 77, pp. 73–80, May 2018.
[30] D. Ahn, J. S. Park, C. S. Kim, J. Kim, Y. Qian, and T. Itoh, "A design of the low-pass filter using the novel microstrip defected ground structure," *IEEE Trans. Microw. Theory Techn.*, vol. 49, no. 1, pp. 86–93, Jan. 2001.
[31] X. Y. Zhang, Q. Xue, C. H. Chan, and B. J. Hu, "Low-loss frequency-agile bandpass filters with controllable bandwidth and suppressed second harmonic," *IEEE Trans. Microw. Theory Techn.*, vol. 58, no. 6, pp. 1557–1564, Jun. 2010.
[32] D.-J. Woo, T.-K. Lee, and J. W. Lee, "Equivalent circuit model for a simple slot-shaped DGS microstrip line," *IEEE Microw. Wireless Compon. Lett.*, vol. 23, no. 9, pp. 447–449, Sep. 2013.
[33] A. Boutejdar, "Design of 5 GHz-compact reconfigurable DGS-bandpass filter using varactor-diode device and coupling matrix technique," *Microw. Opt. Technol. Lett.*, vol. 58, no. 2, pp. 304–309, 2016.
[34] J.-S. Hong, *Microstrip Filters for RF/Microwave Applications*, 2nd ed. New York, NY, USA: Wiley, 2011.
[35] N. Nguyen-Trong, T. Kaufmann, L. Hall, and C. Fumeaux, "Analysis and design of a reconfigurable antenna based on half-mode substrate-integrated cavity," *IEEE Trans. Antennas Propag.*, vol. 63, no. 8, pp. 3345–3353, Aug. 2015.
[36] MuRata Manufacturing. *GRM155R61H104KE19 Capacitance Datasheet*. Accessed: Jun. 15, 2018. [Online]. Available: https://search.murata.co.jp/Ceramy/image/img/A01X/G101/ENG/GRM155R61H104KE19-01A.pdf
[37] A. M. E. Safwat, F. Podevin, P. Ferrari, and A. Vilcot, "Tunable bandstop defected ground structure resonator using reconfigurable dumbbell-shaped coplanar waveguide," *IEEE Trans. Microw. Theory Techn.*, vol. 54, no. 9, pp. 3559–3564, Sep. 2006.
[38] J. Wang, H. Ning, and L. Mao, "A compact reconfigurable bandstop resonator using defected ground structure on coplanar waveguide," *IEEE Antennas Wireless Propag. Lett.*, vol. 11, pp. 457–459, Apr. 2012.

ZHIBIN ZENG received the B.E. degree in information engineering from the Wuhan Technical University of Surveying and Mapping, Wuhan, China, in 1998, the M.E. degrees in information and communication engineering from Xidian University, Xi'an, China, in 2004, and the Ph.D. degrees in electronic science and technology from Xidian University, in 2010, where he has been an Associate Professor with the School of Microelectronics, since 2011. His current research interests include design of embedded systems, wireless communication, high-speed signal processing, and signal integrity.

SHENGJIAN JAMMY CHEN (S'13–M'17) received the B.E. degree in information engineering from the Guangdong University of Technology, Guangzhou, China, in 2003, and the M.E. and Ph.D. degrees in electrical and electronic engineering from The University of Adelaide, Australia, in 2013 and 2017, respectively, where he has been a Postdoctoral Researcher and a Lecturer with the School of Electrical and Electronic Engineering, since 2017.

His current research interests include RFID-based wearable applications, leaky wave antennas, as well as wearable and reconfigurable electromagnetic structures based on novel conductive materials such as graphene, conductive polymers, and conductive fabrics. He has received a number of scholarships, including the Australian Postgraduate Award (2013) and the 2015 Simon Rockliff Scholarship for Outstanding Mentorship. Moreover, he was the recipient of a number of awards, including the Young Scientist Best Paper Award at the International Conference on Electromagnetics in Advanced Applications (ICEAA) 2015, the Young Scientist Best Paper Award and Travel Bursary Award at the International Conference on Electromagnetics in Advanced Applications (ICEAA) 2016, an Honorable Mention at the IEEE AP-S Symposium on Antennas and Propagation (APS/URSI) 2017, and the CST University Publication Award 2017. In addition, his joint paper for the IEEE Radio 2018 received the Best Student Paper Award.

CHRISTOPHE FUMEAUX (M'03–SM'09–F'19) received the Diploma and Ph.D. degrees in physics from ETH Zurich, Switzerland, in 1992 and 1997, respectively.

From 1998 to 2000, he was a Postdoctoral Researcher with the School of Optics, University of Central Florida, Orlando, FL, USA. In 2000, he joined the Swiss Federal Office of Metrology as a Scientific Staff Member. From 2001 to 2008, he was a Research Associate and a Lecturer with the Laboratory for Electromagnetic Fields and Microwave Electronics, ETH Zurich. Since 2008, he has been with The University of Adelaide, where he is currently a Professor with the School of Electrical and Electronic Engineering. His current main research interests concern antenna engineering, THz technology, and the application of RF design principles to optical micro/nano-structures. From 2011 to 2015, he was a Future Fellow of the Australian Research Council. He was a recipient of the ETH Medal for his doctoral dissertation. He was a recipient of the 2018 Edward E. Altshuler Prize, the 2014 IEEE Sensors Journal, and the 2004 ACES Journal Best Paper Awards. He also received the Best Conference Paper Awards at the 2012 Asia-Pacific International Symposium on Electromagnetic Compatibility (APEMC 2012) and the 17th Colloque International sur la Compatibilité Electromagnétique (CEM 2014). More than ten of his students have received student awards with joint papers at the IEEE conferences. He was a recipient of the University of Adelaide Stephen Cole the Elder Award for Excellence in Higher Degree by Research Supervisory Practice, in 2018. He has served as an Associate Editor for the IEEE TRANSACTIONS ON MICROWAVE THEORY AND TECHNIQUES, from 2010 to 2013. From 2013 to 2016, he has served as a Senior Associate Editor, and later an Associate Editor-in-Chief for the IEEE TRANSACTIONS ON ANTENNAS AND PROPAGATION. Since 2017, he has been serving as the Editor-in-Chief for the IEEE ANTENNAS AND WIRELESS PROPAGATION LETTERS.